


Current-induced phonon Hall effect

Kangtai Sun ,* Zhibin Gao , and Jian-Sheng Wang 

Department of Physics, National University of Singapore, Singapore 117551, Republic of Singapore

 (Received 22 May 2020; revised 26 September 2020; accepted 28 September 2020; published 22 October 2020)

Since the first experimental observation of the phonon Hall effect (PHE) in 2005, its physical origin and theoretical explanation have been extensively investigated. While spin-orbit interactions are believed to play important roles under external magnetic fields, nonmagnetic effects are also possible. Here we propose a mechanism of PHE which is induced by electric current in a nonequilibrium system through electron-phonon interactions. The influence of the drift electrons to the phonon degrees of freedom, as a correction to the Born-Oppenheimer approximation, is represented by an antisymmetric matrix which has the same form as in a typical phonon Hall model. We demonstrate the idea with a graphenelike hexagonal lattice having a finite phonon Hall conductivity under a driven electric current.

DOI: [10.1103/PhysRevB.102.134311](https://doi.org/10.1103/PhysRevB.102.134311)

I. INTRODUCTION

The Hall effects, which have been widely studied in electronic systems, are also observed and explained in recent years in phononic systems. The thermal current could also be bent by a magnetic field [1] through Raman-type spin-phonon interactions [2]. As with the integer quantum Hall effect, the phonon Hall effect can be related to the topological nature of the phonon bands [2,3]. More generally, parallel to the Hall effect in electron transport, it was proposed that, as long as there is a gauge potential playing a similar role as the vector potential in a magnetic field, there will be PHE [3]. This net vector potential could come from the inner electron structure of an atomic system itself combined with an external magnetic field [4], which has been observed in very recent experiment [5], or other more complicated interactions like magnon-phonon interactions [6]. All of the present PHEs, either experimental or theoretical, need external [7,8] or internal magnetic field to induce the observable phonon Hall conductivity.

In 2010, Lü *et al.* [9] applied an electric current to a molecular junction and found that the current could break the junction due to a nonconservative force, originated from a Berry phase. This inspires us to think about what could happen if we apply an electric current to a lattice system. Having a current means we have broken the time-reversal symmetry, which in some sense has the same effect as an applied magnetic field. For the Hall conductivity calculation, we follow the modern method of Qin *et al.* [3], which takes into account the so-called energy magnetization contribution, while those of earlier results of Wang and Zhang based on the Green-Kubo formula [10–12] did not realize such a correction. We compute the phonon Hall conductivity and obtain an approximately linear dependence with the drift velocity.

The paper is organized as follows. In Sec. II we introduce a general theory for the PHE and the principle of our current-induced PHE. In Sec. III we demonstrate how we construct our lattice model. In Sec. IV we show our numerical results and discuss their significance. In Sec. V we draw a brief conclusion of our work. We also give an Appendix section which contains some key details.

II. MECHANISM OF PHONON HALL EFFECT

A. Phonon Hall effect under nonzero vector potential

What is the most general form of a Hamiltonian for phonons that can result in a Hall effect? Let us consider a very general system described by $2N$ Hermitian variables y_j , $j = 1, 2, \dots, 2N$, for a system of N degrees of freedom. In column vector notation, we denote this by y , where x components come first, then followed by y components for each degree of freedom. We assume that the Hamiltonian takes a quadratic form of $\hat{H} = \frac{1}{2}y^T H y$, here we assume H is real and symmetric, and superscript T is the matrix transpose. The operators y_j are completely characterized by their commutation relations $[y_j, y_{j'}] = i\hbar J_{jj'}$. We assume that $J_{jj'}$ is a c number. Since y is Hermitian, we can show that the matrix J is real and antisymmetric. The Heisenberg equation of motion is simply

$$\frac{dy}{dt} = JHy. \quad (1)$$

Two common choices of y appear in the literature, that of Zhang *et al.* use conjugate pairs of displacement coordinates u and momenta p , while Qin *et al.* use the displacements u and velocities $v = du/dt = p - Au$. Here in this paper we follow Qin's convention. Then the matrix J takes the following form:

$$J = \begin{pmatrix} 0 & I \\ -I & -2A \end{pmatrix}, \quad \text{with } y = \begin{pmatrix} u \\ v \end{pmatrix}, \quad (2)$$

here the matrix A is antisymmetric.

The effect of the Berry phase was long known in coupled electron-nuclear systems [13], but usually this extra term is

*E0212212@u.nus.edu

neglected in a Born-Oppenheimer approximation. When this term is taken back, the Hamiltonian of the nuclei or phonons in a solid is given by Mead and Truhlar [14]:

$$\hat{H} = \sum_{lj} \frac{[-i\hbar\nabla_{lj} - \mathbf{A}(\mathbf{R})_{lj}]^2}{2M_j} + U(\mathbf{R}), \quad (3)$$

where \mathbf{R}_{lj} is the nucleus position vector of atom j with mass M_j in the unit cell l , and $U(\mathbf{R})$ is the potential on the nuclei. Here the vector potential \mathbf{A} comes from the electron Berry phases but can also be the effect of other interactions such as Raman-type spin-phonon interaction, external magnetic fields [2], or spin-orbit interaction within electronic structure [3]. Throughout this paper, index j for bold symbol stands for atom sites, for unbold symbol, j also includes Cartesian components. In a periodic lattice system with a harmonic approximation, we can transform the system into the reciprocal space, and use a combined coordinate and velocity variable y_q so that $\hat{H} = \frac{1}{2} \sum_q y_q^\dagger H(\mathbf{q}) y_q$. Here \mathbf{q} is the wave vector sampling over the first Brillouin zone. Note that y_q is not a Hermitian operator; it is a vector of smaller dimension varying over twice the degrees of freedom per unit cell for each \mathbf{q} . Elements of the $H(\mathbf{q})$ matrix are determined by y_q . The commutation relation in \mathbf{q} space is [6]

$$[y_{jq}, y_{j'q'}^\dagger] = i\hbar J_{jj'}(\mathbf{q}) \delta_{qq'}. \quad (4)$$

Next by assuming $y_q = \psi_q e^{-i\omega t}$, the corresponding eigen-system of the equation of motion will be

$$iJ(\mathbf{q})H(\mathbf{q})\psi_q \equiv H_{\text{eff}}\psi_q = \omega\psi_q. \quad (5)$$

Since the effective Hamiltonian is non-Hermitian, the left eigenvector is not related by Hermitian conjugate to the right eigenvector. We can choose the left eigenvector as $\tilde{\psi}_q = \psi_q^\dagger H(\mathbf{q})$. The normalization condition is then $\tilde{\psi}_q^\dagger H(\mathbf{q})\psi_q \equiv \tilde{\psi}_q \psi_q = 1$. This eigenequation is general to any possible source of the nonzero vector potential. For example, we can choose $y_q = (\mathbf{u}_q, \mathbf{v}_q)^T$ where $\mathbf{v}_q = \dot{\mathbf{u}}_q$, $\mathbf{u}_{jq} = \sqrt{M_j/N} \sum_l \mathbf{x}_{lj} e^{-i\mathbf{q}\cdot\mathbf{R}_l^0}$ with \mathbf{R}_l^0 being the real space lattice vector, and \mathbf{x}_{lj} being the deviation from equilibrium positions of atom j in cell l . N is the total number of unit cells. We write \mathbf{u}_q without the index j as a column vector consisting of the degrees in a unit cell. Once we have obtained the eigenvalues and associated eigenvectors of the effective Hamiltonian, we can calculate its Berry curvature and phonon Hall conductivity using the formulas given by Qin *et al.* [3],

$$\Omega_{qi} = -\text{Im} \left[\frac{\partial \tilde{\psi}_{qi}}{\partial \mathbf{q}} \times \frac{\partial \psi_{qi}}{\partial \mathbf{q}} \right] \quad (6)$$

and [15]

$$\kappa_{xy} = -\frac{1}{2T} \int_{-\infty}^{\infty} d\epsilon \epsilon^2 \sigma_{xy}(\epsilon) \frac{dn(\epsilon)}{d\epsilon}, \quad (7)$$

where

$$\sigma_{xy}(\epsilon) = -\frac{1}{V\hbar} \sum_{\hbar\omega_{qi} \leq \epsilon} \Omega_{qi}^z, \quad (8)$$

$n(\epsilon) = 1/(e^{\epsilon/(k_B T)} - 1)$ is the Bose function at temperature T , and k_B is the Boltzmann constant. In the above summation over mode qi , all modes with both positive and negative

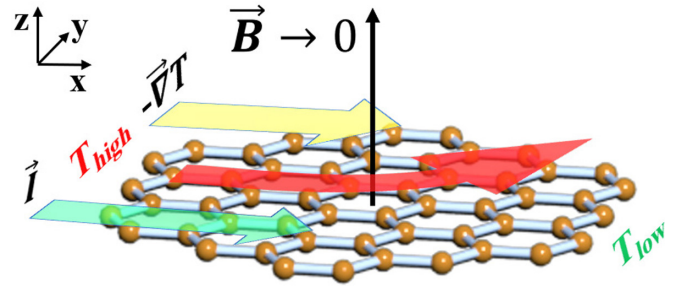


FIG. 1. The schematic setup to detect current-induced phonon Hall effect. Electric current and temperature gradient are needed which are parallel to each other. A very small magnetic field, which is about 10^{-5} T, is to perturb the system and distinguish the direction of the phonon Hall current.

frequencies are included. Since we are dealing with a two-dimensional sheet, the volume V is an ill-defined concept. We use $V = L^2 a$, the area times the thickness, choosing a somewhat arbitrarily to match the units of $\text{W}/(\text{mK})$ of the usual three-dimensional thermal conductivity. When estimating the phonon Hall conductivity κ_{xy} , we assume the thickness of the sample is the same as the bond length $a = 1.42 \text{ \AA}$ of a graphene lattice.

B. Current-induced nonzero vector potential

Lü *et al.* [9] theoretically studied the effect of electric current on a molecular bridge connecting two metallic electrodes. They found a new mechanism, which involves Berry phase, that can lead to a breakdown of the bridge by a “run away” mode. Their discovery inspired us to ask if we introduce electric current into a lattice system, e.g., the honeycomb lattice, is there a phonon Hall effect? The run away mode means the amplitude of oscillation including those perpendicular to the molecular bridge will grow in time, therefore if we extend it to a 2D lattice, this run away mode induced by electric current may result in a phonon Hall current. Figure 1 provides a possible setup on a honeycomb lattice for this current-induced phonon Hall effect.

For convenience, we use the renormalized coordinate $\mathbf{u}_{lj} \equiv \sqrt{M_j} \mathbf{x}_{lj}$ to denote the nucleus displacement in real space. Electrons in a metal or a semiconductor carrying electric current can interact with the lattice phonons through the electron-phonon interaction (EPI). In the NEGF formalism, EPI effect is included as a self-energy term in the phonon retarded Green’s function [16],

$$D(\omega, \mathbf{q}) = [\omega^2 I - \tilde{K}_q - \Pi(\omega=0) - \Pi_q^{\text{NA}}(\omega)]^{-1}, \quad (9)$$

where I is the identity matrix in site space of a unit cell, and \tilde{K}_q is the dynamic matrix. $\Pi(\omega=0)$ is the second term in the equation below. We subtract it off so that the leading contribution is proportional to the frequency ω in the so-called nonadiabatic self-energy due to electrons:

$$\begin{aligned} \Pi_{qj'j}^{\text{NA}}(\omega) &= \frac{1}{N} \sum_{mn} \sum_k g_{mnj}^*(\mathbf{k}, \mathbf{q}) g_{mnj'}(\mathbf{k}, \mathbf{q}) \\ &\times \left[\frac{f_{m\mathbf{k}+\mathbf{q}} - f_{n\mathbf{k}}}{\epsilon_{m\mathbf{k}+\mathbf{q}} - \epsilon_{n\mathbf{k}} - \hbar\omega - i\eta} - \frac{f_{m\mathbf{k}+\mathbf{q}} - f_{n\mathbf{k}}}{\epsilon_{n\mathbf{k}+\mathbf{q}} - \epsilon_{n\mathbf{k}}} \right], \end{aligned} \quad (10)$$

where f is the Fermi function, g is the converted EPI matrix falling in electron mode space and phonon reciprocal space, \mathbf{k} and \mathbf{q} are wave vectors of electrons and phonons, respectively, $\varepsilon_{n\mathbf{k}}$ is the electron dispersion relation, the subscripts m and n indicate the electron bands, and the subscripts j and j' denote the atomic labels in a unit cell including both atom sites and Cartesian directions. The summation is over the first Brillouin zone of the electrons. A small positive η attributes the electrons with a finite lifetime. The self-energy can be computed from a first-principle package.

Alternatively, the movement of the ions can also be described semiclassically by an equation of motion taking into account the effect of the electrons. In real space under a Markov approximation, it takes the form [17]

$$\ddot{\mathbf{u}} = -K\mathbf{u} - 2A\dot{\mathbf{u}}, \quad (11)$$

where K is the spring constant matrix in real space corresponding to the dynamic matrix \tilde{K}_q in reciprocal space, and A can be regarded as the matrix representation of the vector potential induced by EPI which is antisymmetric. Therefore, the phonon Green's function is

$$D(\omega, \mathbf{q}) = [\omega^2 I - \tilde{K}_q + 2i\omega\tilde{A}_q]^{-1}. \quad (12)$$

Comparing the two expressions, if we ignore the higher order terms of ω in $\Pi^{\text{NA}}(\omega)$, and note that \tilde{A}_q is anti-Hermitian [the anti-Hermitian part of $\Pi^{\text{NA}}(\omega)$ is the source of dissipative Joule heating, which we will ignore], we can conclude that

$$\tilde{A}_q = \lim_{\omega \rightarrow 0} \frac{\Pi^{\text{NA}}(\omega) + (\Pi^{\text{NA}})^\dagger(\omega)}{-4i\omega}. \quad (13)$$

The Markov approximation adopted here is well justified as the electrons move on a much faster timescale than that of the nuclear degrees of freedom. In terms of the energy scale, an electron has typical energy of order eV, while phonon $\hbar\omega$ is of the order 100 meV or less. So keeping the leading ω dependence only on self-energy is a good approximation. We can trace back to an effective Hamiltonian for phonons with the electrons taken into account through a nondissipative term as

$$\hat{H} = \frac{1}{2}(p - Au)^2 + \frac{1}{2}u^T Ku, \quad (14)$$

and the corresponding eigenequation is

$$\begin{aligned} \omega\psi_q &= i \begin{pmatrix} 0 & I \\ -I & -2\tilde{A}_q \end{pmatrix} \begin{pmatrix} \tilde{K}_q & 0 \\ 0 & I \end{pmatrix} \psi_q \\ &= \begin{pmatrix} 0 & iI \\ -i\tilde{K}_q & -i2\tilde{A}_q \end{pmatrix} \psi_q. \end{aligned} \quad (15)$$

Here we choose $y_q = (\mathbf{u}_q, \mathbf{v}_q)^T$, and $\mathbf{v}_q = \mathbf{p}_q - \tilde{A}(\mathbf{q})\mathbf{u}_q$ as before.

III. MODEL IMPLEMENTATION ON A GRAPHENELIKE LATTICE

A. Hamiltonians and self-energy

Graphene has been widely studied and it has remarkably high electron mobility, therefore we choose a graphenelike lattice to implement our settings. We use a standard spinless

tight-binding model for the electrons:

$$\hat{H}_e = -t \sum_{l\delta} [c_{A,l}^\dagger c_{B,l+\delta} + c_{B,l}^\dagger c_{A,l+\delta}], \quad (16)$$

where $t = 2.8$ eV is the hopping parameter. A and B indicate the two sublattices, l runs over the Bravais lattice sites, and δ runs over the displacements of the three nearest neighbors of a given site. Zhang *et al.* [2] have proposed a simple phonon model for a graphenelike lattice in which the coupling matrix is diagonal when the bond orientation is in the x direction between two atoms,

$$K_x = \begin{pmatrix} K_L & 0 \\ 0 & K_T \end{pmatrix}, \quad (17)$$

where $K_L = 0.144$ eV/(uÅ²) is the longitudinal spring constant and $K_T = K_L/4$ is the transverse spring constant. Other orientations can be obtained by rotations. The dynamic matrix is given by

$$\tilde{K}_q = \sum_{l'l'} K_{l'l'} e^{i(\mathbf{R}_{l'}^0 - \mathbf{R}_l^0) \cdot \mathbf{q}}, \quad (18)$$

where $K_{l'l'}$ is the submatrix between unit cell l and l' in the full K . In this model we have ignored the z mode and consider only the in-plane motion. The reason is that the motion in the direction perpendicular to the plane couples quadratically to the electron degrees of freedom, and this is a high order effect to the electron-phonon interaction.

For the electron-phonon interaction, we take a Su-Schrieffer-Heeger-like model, as used in a previous work by Jiang and Wang [18],

$$\begin{aligned} \hat{H}_{\text{epi}} &= J_1 \sum_{l\delta} [c_{A,l}^\dagger c_{B,l+\delta} + c_{B,l+\delta}^\dagger c_{A,l}] \\ &\quad \times [(\mathbf{u}_{B,l+\delta} - \mathbf{u}_{A,l}) \cdot \hat{\mathbf{e}}_{l,\delta}], \end{aligned} \quad (19)$$

where $J_1 = -6.0$ eV/Å and $\hat{\mathbf{e}}_{l,\delta}$ is the direction between two nearest atoms. The g matrix is given by

$$g_{mnj}(\mathbf{k}, \mathbf{q}) = \sum_{m'n'} S_{mm'}^\dagger(\mathbf{k} + \mathbf{q}) \Xi_{m'n'}^j(\mathbf{k}, \mathbf{q}) S_{n'n}(\mathbf{k}), \quad (20)$$

where $j = \{Ax, Ay, Bx, By\}$,

$$S(\mathbf{k}) = \frac{1}{\sqrt{2}} \begin{pmatrix} 1 & e^{i\phi(\mathbf{k})} \\ -e^{-i\phi(\mathbf{k})} & 1 \end{pmatrix}, \quad (21)$$

with $e^{i\phi(\mathbf{k})} = f(\mathbf{k})/|f(\mathbf{k})|$, $f(\mathbf{k}) = e^{-ik_x a} + e^{i(k_x a/2 + \sqrt{3}k_y a/2)} + e^{i(k_x a/2 - \sqrt{3}k_y a/2)}$, and $\Xi_{m'n'}^j(\mathbf{k}, \mathbf{q})$ is the reciprocal EPI matrix corresponding to \hat{H}_{epi} . The expression is given in Appendix A.

In this work we focus on the EPI for \mathbf{k} points near the Dirac points of the electrons and \mathbf{q} near the Γ point of the phonons, for we find that they are dominant in determining the final phonon Hall conductivity. It seems that we have prepared all the ingredients to calculate \tilde{A}_q . However, there is a problem that when we apply an electric current to this graphenelike two-dimensional surface, assuming the drift velocity v_1 of current is along the x direction, it is in a nonequilibrium state, therefore we cannot just substitute the Fermi function into the formula. To solve this problem, we use a single-mode

relaxation approximation [19] so that

$$f = f^0 - \frac{\partial f^0}{\partial \varepsilon} \Phi \approx f^0(\varepsilon - \Phi), \quad (22)$$

where $f^0 = [e^{(\varepsilon - \mu)/k_B T} + 1]^{-1}$ with μ being the chemical potential of electron, and $\Phi \equiv \Phi_{nk}$ is mode dependent:

$$\Phi_{nk} = -eE\tau_{nk} \frac{\partial \varepsilon_{nk}}{\partial \hbar k_x}, \quad (23)$$

where E is the applied electric field, and τ_{nk} is the relaxation time which is only related to the magnitude of the wave vector. In practice, since we do not know the relaxation time, we combine it with the electric field and replace them with the drift velocity v_1 , for graphenelike lattice [20]:

$$\Phi_{nk} = v_1 \operatorname{Re} \left[z^* \frac{\partial z}{\partial k_x} \right] / (\hbar v_F^2), \quad (24)$$

where $v_F = 3at/(2\hbar)$ is the Fermi velocity, $a = 1.42 \text{ \AA}$ is the distance between atoms, and $z = -t f(\mathbf{k})$. By requiring this correction to the Fermi function, the self-energy can be numerically calculated, and thereafter, the \tilde{A}_q matrix.

B. The Berry curvature—is it unique?

As we have discussed in the previous section, the choice of y_q is not unique—at least three different choices exist in the literature. Zhang *et al.* choose $y_q = (u_q, p_q)$, Qin *et al.* choose $y_q = (u_q, v_q)$, and Liu *et al.* choose $y_q = (\tilde{K}_q^{-1/2} u_q, v_q)$ [2,3,21]. The difference between Zhang's and Qin's choices is like the difference between Lagrangian mechanics and Hamiltonian mechanics, therefore they are more or less equivalent. The special choice of Liu results in a Hermitian effective Hamiltonian, which implies immediately the eigenfrequencies are all real. When the vector potential term can be separated from the usual potential energy term as in our case, these three bases are related by similarity transformations explicitly. However, this kind of variable transformations is not gauge invariant. Therefore, generally, if \tilde{A}_q is not a constant matrix, they will result in different Berry curvatures. The question then arises as which one should be used to compute the phonon Hall conductivity? To illustrate and confirm that there is indeed a difference, we choose a smooth $\tilde{A}_q = (\Lambda + i|\Lambda|) * (\mathbf{b} \cdot \mathbf{q} + c)$ matrix, where Λ is a constant 4×4 antisymmetric matrix, $|\Lambda|$ takes the absolute value of each element in Λ , \mathbf{b} is a constant vector parameter, and c is another constant parameter. In principle, these three bases should result in different Berry curvatures, but in practice, the differences are small, especially between Zhang's and Qin's choices, therefore we choose such a highly anisotropic case. We plot the corresponding Berry curvatures of the three bases along a high-symmetry path of the graphenelike lattice in Fig. 2. We see that there are sharp peaks at the Γ point. However, the signs of the peaks are opposite for Liu *et al.* definition to that of Zhang and Qin *et al.* Away from the Γ point, the values tend to be close among the three. In conclusion, since only Qin *et al.* derived the correct formula for the phonon Hall conductivity with their definition of the Berry curvature, which considers an energy magnetization contribution to Hall conductivity [3] while Zhang *et al.* did not, we prefer to follow

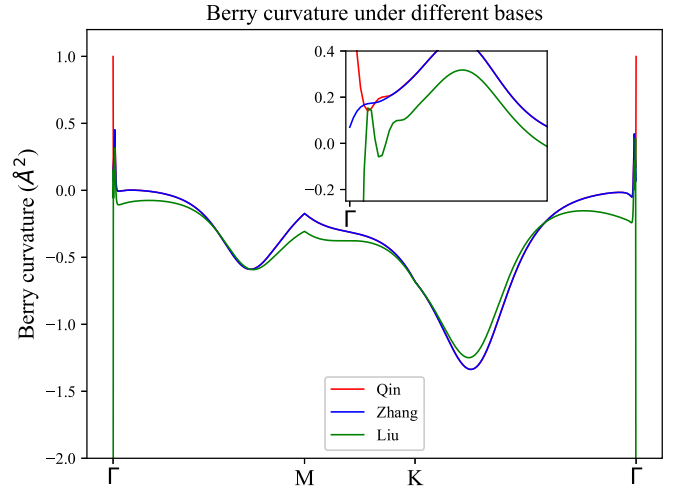


FIG. 2. The Berry curvatures along the high-symmetry path under three different bases [2,3,21]. Although they do not differ so much from each other, they are indeed different. The parameter set is chosen to be: $\mathbf{b} \cdot \mathbf{q} = (1000 \text{ \AA}, 1 \text{ \AA}) \cdot \mathbf{q}$, $c = 0.1 \text{ rad/ps}$, and Λ is a constant antisymmetric matrix with upper triangular elements, lower triangular elements, and diagonal elements being 1.0, -1.0 , and 0 rad/ps , respectively.

Qin's definition. It is natural that if we use other choices, we will obtain different formulas for phonon Hall conductivity.

IV. NUMERICAL RESULTS AND DISCUSSION

In order to have a well-defined topological structure, we need to perturb our system to open tiny gaps at Γ and K points, as the Berry curvature becomes ill-defined when the bands are degenerate. This goal is achieved by adding a small on-site potential term to the phonon dynamic matrix and a nearly zero magnetic field which goes into the Hamiltonian through Raman-type spin-phonon interaction [2]. The effect of the magnetic field is described by a constant antisymmetric matrix A_h :

$$A_h = \begin{pmatrix} B_h & 0 \\ 0 & B_h \end{pmatrix}, \quad B_h = \begin{pmatrix} 0 & h \\ -h & 0 \end{pmatrix}, \quad (25)$$

where h is an effective parameter representing magnetic field with units rad/ps ($1 \text{ rad/ps} \approx 33.3 \text{ cm}^{-1}$). Adding this matrix to our previous \tilde{A}_q will introduce magnetic field into our system. When we calculate \tilde{A}_q , a $400 \times 400 \mathbf{k}$ grid is used and the parameter η is set to be about 0.2 eV . We note that as a function of a constant magnetic field h , the Berry curvatures and the Chern numbers are odd functions of h and experience a discontinuity at $h = 0$, thus ill-defined at $h = 0$. Our results presented below should be considered as the limit when $h \rightarrow 0^+$ and $V_{\text{on-site}} \rightarrow 0^+$. This is physical since we can always apply a small magnetic field and put the system on a substrate, thereby acquiring an on-site interaction. There is one more important thing to note that inside the formula of \tilde{A}_q , since we only focus on \mathbf{q} points near Γ point, there is a hidden δ function behavior when temperature is low. This δ function originates from the difference of the intraband Fermi functions in the numerator of \tilde{A}_q if we take a Taylor expansion of \mathbf{q} near Γ point at low temperature. To handle this

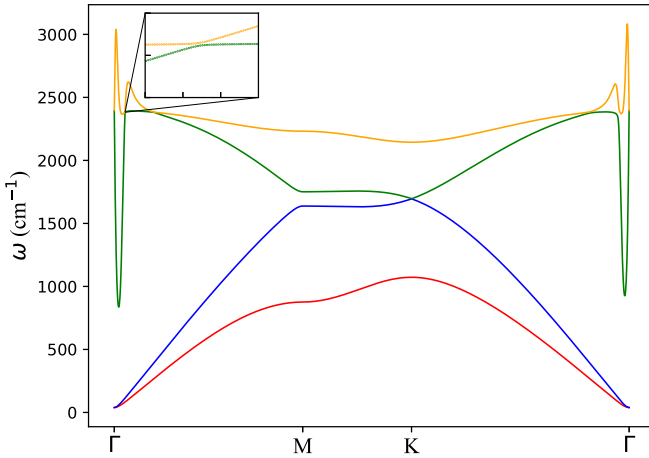


FIG. 3. The dispersion relation of positive branches along high-symmetry path Γ - M - K - Γ with $v_1 = 1.0 \times 10^4$ m/s, $T = 300$ K, $\mu = 0.1$ eV. A small on-site potential $V_{\text{on-site}} = 1.0 \times 10^{-3} K_L$ and a nearly 0 magnetic field measured by effective parameter $h = 1.0 \times 10^{-9}$ rad/ps are employed to perturb the system. The inset shows one of the anticrossing points. Note that the out-of-plane ZA mode is not considered here.

δ function numerically, we should compute in a very dense k grids which requires a lot of computation power. However, we can also broaden this δ function by tuning the electron parameter $\beta = 1/k_B T$. Through computation we find that the differences of EPI at low temperature range, e.g., below 300 K or even below 500 K, are very small, therefore, when we calculate \tilde{A}_q at low temperature, we can make an approximation to fix the broadening parameter to be the value at higher temperature like 300 or 500 K.

Figure 3 shows the positive part of the dispersion relation of our current-induced system, from which we can see that the two acoustic branches are very close to the pure phonon system without the drift current, while the two optical branches get modified drastically. This behavior is easy to understand if we review the EPI form of our model. The strength of EPI in our model is proportional to the relative displacement of atoms, therefore the optical modes, in which atoms move relatively, are equipped with stronger EPI than acoustic ones. It deserves notice that there are several anticrossing points in the dispersion relations. These points will possess much larger Berry curvature, therefore they are dominant in determining the topological properties of the system. Points in acoustic branches near Γ point and anticrossing points near K points also have large Berry curvatures. However, these pairs of Berry curvatures should cancel each other for they are similar to pure phonon system where there are no PHE.

Figure 4(a) demonstrates the relationship between κ_{xy} and the drift velocity v_1 . κ_{xy} is roughly linear dependent on v_1 for our picked velocity sequence. When v_1 is gradually close to the Fermi velocity of this graphenelike lattice system, our theory and approximation on EPI will gradually break down. The Chern numbers of positive branches are $C^1 = 1$, $C^2 = C^3 = 0$, $C^4 = -1$, where larger indices are associated with higher frequencies. In our range of the drift velocity, there is no jump among Chern numbers, which seems kind of trivial. The discontinuities due to numerical errors for the

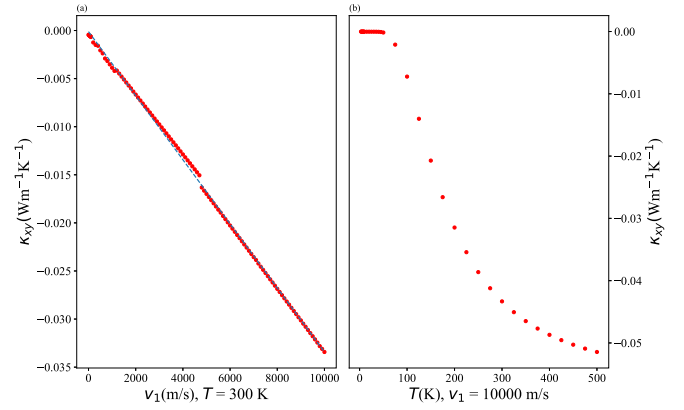


FIG. 4. (a) Phonon Hall conductivity κ_{xy} versus drift velocity v_1 at a temperature $T = 300$ K. The broadening parameter is $\beta = 1/(k_B \times 300 \text{ K})$. (b) Phonon Hall conductivity κ_{xy} versus temperature at $v_1 = 10000$ m/s. The broadening parameter is set to be $\beta = 1/(k_B \times 500 \text{ K})$. These two plots share the same set of parameters of temperature, chemical potential, on-site potential, and nearly 0 magnetic field as Fig. 3.

Chern numbers do not change, which means the dispersion relation of the system has the same pattern. Figure 4(b) shows temperature dependence of κ_{xy} . When the temperature is very small, PHE tends to disappear, and in our temperature range, the absolute value of the phonon Hall conductivity gradually increases as temperature is increasing, but we cannot conclude what the exact relationship between κ_{xy} and temperature is. In our calculation, numerical errors mainly come from the calculation of $\tilde{A}(\mathbf{q})$ and cubic interpolation to obtain its values with denser grids, which is 2000×2000 .

The order of magnitude of our current-induced κ_{xy} is one order smaller than the case with the magnetic field parameter h being several rad/ps. It is instructive to compare the magnitude of the Hall conductivity to the universal conductance quantum which is $G_0 = T(\pi k_B)^2/(3h)$, when converted into the same units of conductivity G_0/a at 300 K, we find it is about 2 W/(mK). Our result is about 1/100th of the conductance quantum. Since κ_{xy} with our model is only about one order smaller than a pure magnetic field experimental results [1], it should be still observable experimentally in principle.

Figure 5 shows this sign jump of the phonon Hall conductivity. The role small magnetic field played in our system is to perturb our system at Γ point to induce circular polarization like the run away mode in the work by Lü *et al.*, for the current-induced $\tilde{A}(\mathbf{q})$ it is 0 due to the translational symmetry. Therefore, the magnetic field determines the sign of the phonon Hall conductivity. Away from Γ point, current-induced $\tilde{A}(\mathbf{q})$ starts to affect the system so that there is a discontinuity of κ_{xy} . In Sec. II we said we ignore the Joule heating effect. However, in practice, Joule heating always exists without special flowing direction. Therefore, it will not prevent us from observing PHE. We simply prepare a sample with temperature gradient in a direction, let electric current flow parallel to this temperature gradient, and apply a small magnetic field twice with opposite direction, then measure the temperature differences in the direction transverse to the

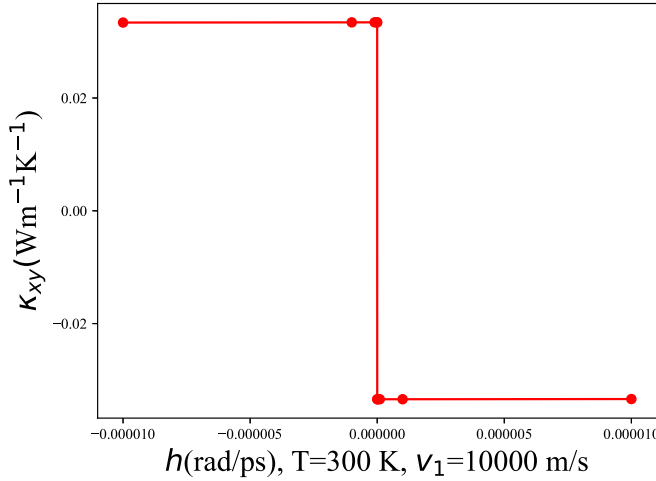


FIG. 5. Phonon Hall conductivity κ_{xy} versus magnetic field parameter h . We can see κ_{xy} changes sign as h changes sign and there is a discontinuity when h crosses 0.

current flow. The Joule heating effect does not change sign while the Hall effect changes sign. From this we can deduce the pure Hall contribution.

V. CONCLUSION

In summary, we have proposed a mechanism of PHE induced by the electric current. Compared with other PHEs, no significant magnetic field is needed in our system. The Chern numbers of some phonon branches are not 0, but the total Chern number of all the branches are still 0. The property of our system is that for a suitable range of the drift velocities, the phonon Hall conductivity has a linear relation on the drift velocity, which is proportional to the applied current.

ACKNOWLEDGMENTS

We thank Professor Jingtao Lü and Professor Lifa Zhang for discussions. J.-S.W. is supported by a FRC Grant R-144-000-402-114 and an MOE tier 2 Grant R-144-000-411-112. Z.G. acknowledges the financial support from FRC funding of Singapore (Grant No. R-144-000-402-114).

APPENDIX A: DYNAMIC MATRIX AND EPI MATRIX ELEMENTS

Starting from a basic coupling matrix between two atoms in x direction K_x , we can construct a dynamic matrix of our lattice model [2]. In our coordinates, unit cell lattice vectors are $\mathbf{a}_1 = (3a/2, \sqrt{3}a/2)$ and $\mathbf{a}_2 = (3a/2, -\sqrt{3}a/2)$. The explicit coupling matrices among three nearest pair can be obtained by a rotation matrix U which are $K_{01} = U(\pi/3)K_xU(-\pi/3)$, $K_{02} = U(-\pi/3)K_xU(\pi/3)$, and $K_{03} = U(\pi)K_xU(-\pi)$, respectively. Based on these matrices, we can construct five coupling matrices between unit cells:

$$K_0 = \begin{pmatrix} K_{01} + K_{02} + K_{03} & -K_{03} \\ -K_{03} & K_{01} + K_{02} + K_{03} \end{pmatrix}, \quad (A1)$$

$$K_1 = \begin{pmatrix} 0 & 0 \\ -K_{02} & 0 \end{pmatrix}, \quad K_2 = \begin{pmatrix} 0 & 0 \\ -K_{01} & 0 \end{pmatrix}, \quad (A2)$$

$$K_3 = \begin{pmatrix} 0 & -K_{02} \\ 0 & 0 \end{pmatrix}, \quad K_4 = \begin{pmatrix} 0 & -K_{01} \\ 0 & 0 \end{pmatrix}. \quad (A3)$$

Then the dynamic matrix is

$$\begin{aligned} \tilde{K}_q &= K_0 + K_1 e^{i(3q_x a/2 - \sqrt{3}q_y a/2)} + K_2 e^{i(3q_x a/2 + \sqrt{3}q_y a/2)} \\ &+ K_3 e^{-i(3q_x a/2 - \sqrt{3}q_y a/2)} + K_4 e^{-i(3q_x a/2 + \sqrt{3}q_y a/2)}. \end{aligned} \quad (A4)$$

To calculate the nonadiabatic self-energy Π_q^{NA} , we need to know EPI matrix in reciprocal space. By transforming \hat{H}_{epi} into reciprocal space, we can extract tensor elements. We use A,B to represent two atoms in a unit cell and {Ax, Ay, Bx, By} to represent four degrees of freedom of EPI in our lattice model. Then the reciprocal EPI matrix elements are

$$\Xi_{\text{AB}}^{\text{Ax}}(\mathbf{k}, \mathbf{q}) = -J_1 [e^{ik_x a/2} \cos(\sqrt{3}k_y a/2) - e^{-ik_x a}], \quad (A5)$$

$$\Xi_{\text{AB}}^{\text{Ay}}(\mathbf{k}, \mathbf{q}) = -J_1 \sqrt{3} i e^{ik_x a/2} \sin(\sqrt{3}k_y a/2), \quad (A6)$$

$$\Xi_{\text{AB}}^{\text{Bx}}(\mathbf{k}, \mathbf{q}) = J_1 \{e^{i(k_x + q_x) a/2} \cos[\sqrt{3}(k_y + q_y) a/2] - e^{-i(k_x + q_x) a}\}, \quad (A7)$$

$$\Xi_{\text{AB}}^{\text{By}}(\mathbf{k}, \mathbf{q}) = J_1 \sqrt{3} i e^{i(k_x + q_x) a/2} \sin[\sqrt{3}(k_y + q_y) a/2], \quad (A8)$$

$$\Xi_{\text{BA}}^j(\mathbf{k}, \mathbf{q}) = [\Xi_{\text{AB}}^j(\mathbf{k} + \mathbf{q}, -\mathbf{q})]^*, \quad j = \{\text{Ax}, \text{Ay}, \text{Bx}, \text{By}\}, \quad (A9)$$

and other elements are all zero.

APPENDIX B: EQUATION OF MOTION CONTAINING A MATRIX

For a general electron-phonon system, there is a generalized Langevin equation describing the atoms' movement [17]:

$$\ddot{\mathbf{u}} = -K\mathbf{u} - \int^t \Pi_{\text{epi}}^r(t-t')\mathbf{u}(t')dt' + \xi. \quad (B1)$$

Here we do not consider the bath contribution and set the noise term ξ to zero, for our system is infinitely large. We can define $d\Gamma(t)/dt \equiv \Pi_{\text{epi}}^r(t)$ and integrate by parts so that the equation of motion becomes

$$\ddot{\mathbf{u}} = -K\mathbf{u} - \int^t \Gamma(t-t')\dot{\mathbf{u}}(t')dt'. \quad (B2)$$

Next we apply a Markov approximation to $\Gamma(t-t')$ so that $\Gamma(t-t') \approx 4A(t')\delta(t-t')$ (factor 4 is for consistency). The final expression of the equation of motion will be

$$\ddot{\mathbf{u}} = -K\mathbf{u} - 2A\dot{\mathbf{u}}, \quad (B3)$$

which is used in Sec. II.

APPENDIX C: BERRY CURVATURE

Usually there are two ways of calculating the Berry curvature, one is the explicit way by inserting the completeness identity into the definition of the Berry curvature. In our system, the explicit formula is

$$\Omega_i = -\text{Im} \sum_{i' \neq i} \frac{\tilde{\psi}_i \frac{\partial H_{\text{eff}}}{\partial q_x} \psi_{i'} \tilde{\psi}_{i'} \frac{\partial H_{\text{eff}}}{\partial q_y} \psi_i - (q_x \leftrightarrow q_y)}{(\omega_i - \omega_{i'})^2}. \quad (C1)$$

However, to calculate the partial derivative of H_{eff} , we need numerical differentiation which will cost a large amount of computation to be precise enough. Therefore we choose another way, a geometric way by dividing the Brillouin zone into plaquettes each consisting of four points on a square with area ΔS and calculating the Berry phase around them [22,23]:

$$\phi = -\text{Im} \ln(\bar{\psi}_1 \psi_2 \bar{\psi}_2 \psi_3 \bar{\psi}_3 \psi_4 \bar{\psi}_4 \psi_1). \quad (\text{C2})$$

Compared with the Hermitian case, we have replaced the Hermitian conjugate of the eigenvector by the left eigenvector. If investigated further, we find that this replacement is not correct for $\bar{\psi}_1 \psi_2 \neq (\bar{\psi}_2 \psi_1)^*$. This break of the equality, a fundamental property of the inner product in Hilbert space,

will invalidate Stokes' theorem so that we cannot obtain Berry curvature through Berry phase. To overcome this, we define a new version of inner product:

$$\langle \bar{\psi}_1 \psi_2 \rangle \equiv \frac{\bar{\psi}_1 \psi_2 + (\bar{\psi}_2 \psi_1)^*}{2}. \quad (\text{C3})$$

With this definition, property of inner product in Hilbert space and validity of Stokes' theorem are restored. Then the Berry curvature is calculated by

$$\Omega = \lim_{\Delta S \rightarrow 0} \frac{-\text{Im} \ln(\langle \bar{\psi}_1 \psi_2 \rangle \langle \bar{\psi}_2 \psi_3 \rangle \langle \bar{\psi}_3 \psi_4 \rangle \langle \bar{\psi}_4 \psi_1 \rangle)}{\Delta S}. \quad (\text{C4})$$

One can show that the two ways computing the Berry curvature are mathematically equivalent.

-
- [1] C. Strohm, G. L. J. A. Rikken, and P. Wyder, Phenomenological Evidence for the Phonon Hall Effect, *Phys. Rev. Lett.* **95**, 155901 (2005).
- [2] L. Zhang, J. Ren, J.-S. Wang, and B. Li, Topological Nature of the Phonon Hall Effect, *Phys. Rev. Lett.* **105**, 225901 (2010).
- [3] T. Qin, J. Zhou, and J. Shi, Berry curvature and the phonon Hall effect, *Phys. Rev. B* **86**, 104305 (2012).
- [4] T. Saito, K. Misaki, H. Ishizuka, and N. Nagaosa, Berry Phase of Phonons and Thermal Hall Effect in Nonmagnetic Insulators, *Phys. Rev. Lett.* **123**, 255901 (2019).
- [5] X. Li, B. Fauqué, Z. Zhu, and K. Behnia, Phonon Thermal Hall Effect in Strontium Titanate, *Phys. Rev. Lett.* **124**, 105901 (2020).
- [6] X. Zhang, Y. Zhang, S. Okamoto, and D. Xiao, Thermal Hall Effect Induced by Magnon-Phonon Interactions, *Phys. Rev. Lett.* **123**, 167202 (2019).
- [7] B. K. Agarwalla, L. Zhang, J.-S. Wang, and B. Li, Phonon Hall effect in ionic crystals in the presence of static magnetic field, *Euro. Phys. J. B* **81**, 197 (2011).
- [8] J.-Y. Chen, S. A. Kivelson, and X.-Q. Sun, Enhanced Thermal Hall Effect in Nearly Ferroelectric Insulators, *Phys. Rev. Lett.* **124**, 167601 (2020).
- [9] J.-T. Lü, M. Brandbyge, and P. Hedegård, Blowing the fuse: Berry's phase and runaway vibrations in molecular conductors, *Nano Lett.* **10**, 1657 (2010).
- [10] J.-S. Wang and L. Zhang, Phonon Hall thermal conductivity from the Green-Kubo formula, *Phys. Rev. B* **80**, 012301 (2009).
- [11] L. Sheng, D. N. Sheng, and C. S. Ting, Theory of the Phonon Hall Effect in Paramagnetic Dielectrics, *Phys. Rev. Lett.* **96**, 155901 (2006).
- [12] Y. Kagan and L. A. Maksimov, Anomalous Hall Effect for the Phonon Heat Conductivity in Paramagnetic Dielectrics, *Phys. Rev. Lett.* **100**, 145902 (2008).
- [13] C. A. Mead, The geometric phase in molecular systems, *Rev. Mod. Phys.* **64**, 51 (1992).
- [14] C. A. Mead and D. G. Truhlar, On the determination of Born-Oppenheimer nuclear motion wave functions including complications due to conical intersections and identical nuclei, *J. Chem. Phys.* **70**, 2284 (1979).
- [15] L. Zhang, Berry curvature and various thermal Hall effects, *New J. Phys.* **18**, 103039 (2016).
- [16] F. Giustino, Electron-phonon interactions from first principles, *Rev. Mod. Phys.* **89**, 015003 (2017).
- [17] J.-T. Lü, H. Zhou, J.-W. Jiang, and J.-S. Wang, Effects of electron-phonon interaction on thermal and electrical transport through molecular nano-conductors, *AIP Adv.* **5**, 053204 (2015).
- [18] J.-W. Jiang and J.-S. Wang, Joule heating and thermoelectric properties in short single-walled carbon nanotubes: Electron-phonon interaction effect, *J. Appl. Phys.* **110**, 124319 (2011).
- [19] J. M. Ziman, *Electrons and Phonons: The Theory of Transport Phenomena in Solids* (Oxford University Press, Oxford, 2001).
- [20] J. Peng and J.-S. Wang, Current-induced heat transfer in double-layer graphene, [arXiv:1805.09493](https://arxiv.org/abs/1805.09493).
- [21] Y. Liu, Y. Xu, S.-C. Zhang, and W. Duan, Model for topological phononics and phonon diode, *Phys. Rev. B* **96**, 064106 (2017).
- [22] T. Fukui, Y. Hatsugai, and H. Suzuki, Chern numbers in discretized Brillouin zone: Efficient method of computing (spin) Hall conductances, *J. Phys. Soc. Jpn.* **74**, 1674 (2005).
- [23] D. Vanderbilt, *Berry Phases in Electronic Structure Theory: Electric Polarization, Orbital Magnetization and Topological Insulators* (Cambridge University Press, Cambridge, 2018).